AGU PUBLICATIONS

Geophysical Research Letters

RESEARCH LETTER
10.1002/2016GL070723

Key Points:
- Decreased surface-intermediate ocean $\delta^{13}C$ gradients suggest that the biological pump weakened during HS1 and the YD
- Weakened AMOC during HS1 likely altered the global nutrient budget, decreased biological pump efficiency, and led to CO_2 rise
- Proxy records are inconsistent with entrainment of light carbon in AAIW/SAMW during HS1

Supporting Information:
- Supporting Information S1

Correspondence to:
J. E. Hertzberg,
jennifer.hertzberg@uconn.edu

Citation:
Hertzberg, J. E., D. C. Lund, A. Schmittner, and A. L. Skrivanek (2016), Evidence for a biological pump driver of atmospheric CO_2 rise during Heinrich Stadial 1, *Geophys. Res. Lett.*, *43*, doi:10.1002/2016GL070723.

Received 4 AUG 2016
Accepted 4 NOV 2016
Accepted article online 9 NOV 2016

Evidence for a biological pump driver of atmospheric CO_2 rise during Heinrich Stadial 1

Jennifer E. Hertzberg[1], David C. Lund[1], Andreas Schmittner[2], and Alexandra L. Skrivanek[3]

[1]Department of Marine Sciences, University of Connecticut, Groton, Connecticut, USA, [2]College of Earth, Ocean, and Atmospheric Sciences, Oregon State University, Corvallis, Oregon, USA, [3]Department of Geological Sciences, University of Florida, Gainesville, Florida, USA

Abstract The initial trigger of the atmospheric CO_2 rise during Heinrich Stadial 1 (HS1: 14.5–17.5 kyr B.P.) remains elusive. We present a compilation of four paired surface and intermediate-depth foraminiferal $\delta^{13}C$ records to test whether reduced biological pump efficiency led to the initial CO_2 rise during the last deglaciation. Surface ocean $\delta^{13}C$ decreased across HS1 while intermediate-depth $\delta^{13}C$ increased, leading to a reduction in the upper ocean $\delta^{13}C$ gradient. Our compilation also suggests the $\delta^{13}C$ gradient increased during the Bølling-Allerød (12.9–14.5 kyr B.P.) and decreased during the Younger Dryas (YD: 11.7–12.9 kyr B.P.). The HS1 and YD data are consistent with reduced biological export of isotopically light carbon from the surface ocean and its remineralization at depth. Our results support the idea that a weaker Atlantic Meridional Overturning Circulation decreased biological pump efficiency by increasing the overall fraction of preformed nutrients in the global ocean, leading to an increase in atmospheric CO_2.

1. Introduction

The last glacial termination was characterized by an ~30 ppmv increase in atmospheric CO_2 during Heinrich Stadial 1 (HS1: 14.5–17.5 kyr B.P.) [*Marcott et al.*, 2014]. Coincident with the rise in CO_2, the $\delta^{13}C$ of atmospheric CO_2 ($\delta^{13}C$-CO_2) decreased by ~0.3‰, implying that the carbon was sourced from a ^{13}C-depleted reservoir [*Schmitt et al.*, 2012; *Bauska et al.*, 2016]. Keeling plot analyses of the $\delta^{13}C$-CO_2 record from Taylor Glacier, Antarctica, suggest the HS1 rise in atmospheric CO_2 was driven by a weakening of the biological pump [*Bauska et al.*, 2016]. *Bauska et al.* [2016] attribute the weaker biological pump to a decrease in dust delivery to the Southern Ocean and/or enhanced upwelling of deep water in the Southern Ocean. However, a slowdown of the Atlantic Meridional Overturning Circulation (AMOC) can also trigger weakening of the biological pump, an increase in atmospheric CO_2, and a decrease in $\delta^{13}C$-CO_2 [*Ito and Follows*, 2005; *Schmittner and Lund*, 2015]. Multiple paleoceanographic proxies are consistent with weakening of the AMOC during HS1 [*McManus et al.*, 2004; *Gherardi et al.*, 2009; *Oppo et al.*, 2015], suggesting that an associated decrease in biological pump efficiency is a viable driver of the atmospheric CO_2 rise [*Schmittner and Galbraith*, 2008; *Schmittner and Lund*, 2015].

Biological pump efficiency can be assessed using the preformed and regenerated components of the nutrient phosphate. North Atlantic Deep Water (NADW) is sourced from phosphate-depleted surface waters, and thus has low preformed phosphate (Figure S1 in the supporting information). Conversely, Antarctic Bottom Water (AABW) is formed from waters with a high preformed phosphate concentration due to incomplete nutrient utilization in the Southern Ocean. NADW and AABW therefore represent contrasting levels of efficiency for sequestering CO_2 in the abyssal ocean. Low preformed phosphate in NADW indicates that the biological pump has efficiently removed carbon and phosphate from the surface waters in the Atlantic. For AABW, high preformed phosphate represents a missed opportunity for biological productivity to sequester CO_2 in the abyss. As outlined in *Ito and Follows* [2005], both simple theory and modeling results suggest that there is a nearly linear relationship between the fraction of preformed phosphate in the global ocean and atmospheric CO_2 (Figure S1). If AABW becomes a greater fraction of the deep ocean, the overall efficiency of the biological pump decreases and atmospheric CO_2 rises. Weakening of the AMOC during HS1 would therefore reduce the influence of NADW, increase the global mean fraction of preformed phosphate, and cause atmospheric CO_2 levels to increase [*Schmittner and Galbraith*, 2008; *Schmittner and Lund*, 2015]. Note that this manuscript is focused on millennial-scale atmospheric CO_2 variability; additional mechanisms, such as upwelling of carbon from the abyss [*Anderson et al.*, 2009] or variable iron fertilization in the Southern Ocean [*Galbraith and Jaccard*, 2015], are required to account for the full glacial-interglacial CO_2 change.

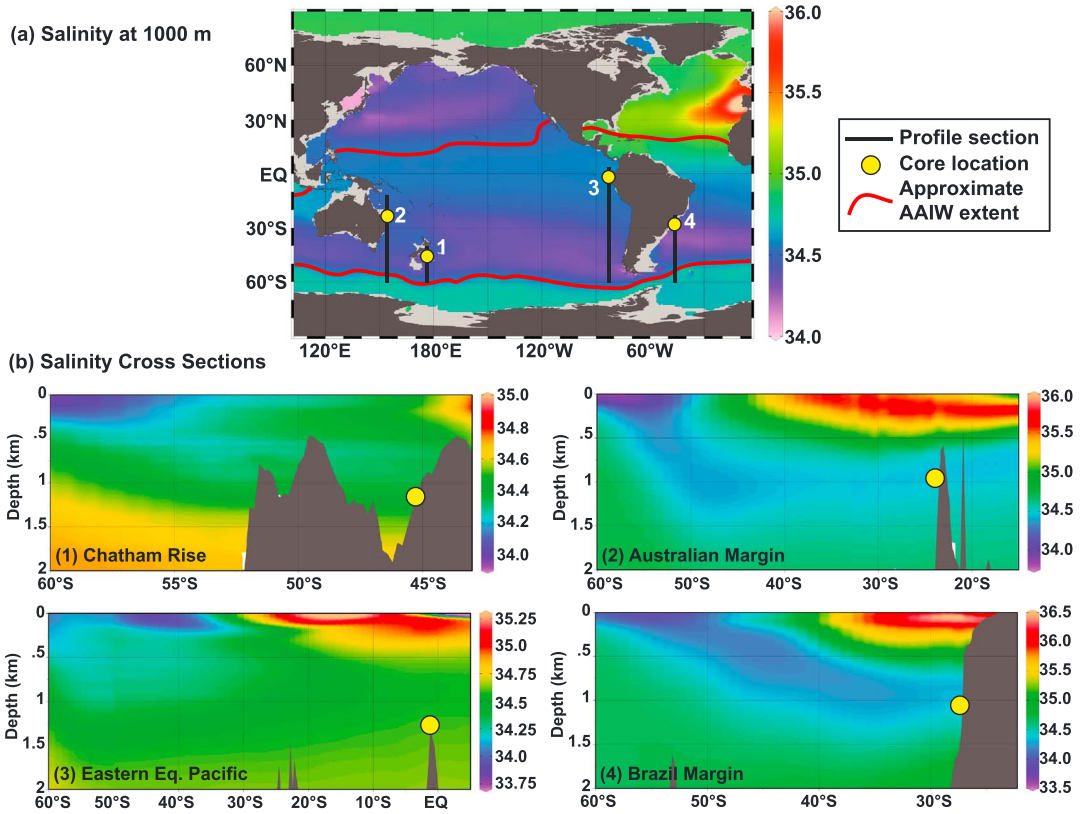

Figure 1. Locations of the sediment cores utilized in this study. (a) Core locations shown in yellow circles on a map of salinity at 1000 m water depth. Numbers correspond to locations listed in Table 1. The approximate extent of AAIW is outlined in red (after *Talley* [2008]). The black lines show the locations of salinity cross sections. (b) Salinity cross sections for the four core locations, including the Chatham Rise (1), Australian Margin (2), Eastern Equatorial Pacific (3), and the Brazil margin (4). Note the location of the sediment cores (in yellow circles) in relation to AAIW, the low salinity water mass sourced from the surface Southern Ocean. Map and cross sections were created with Ocean Data View (https://odv.awi.de) using World Ocean Atlas 13 annually-averaged data [*Zweng et al.*, 2013]. Note that the salinity scales are different for each cross section.

In this study, we test the hypothesis that millennial-scale changes in the AMOC drove variable biological pump efficiency by using reconstructions of surface and intermediate $\delta^{13}C$ of dissolved inorganic carbon (DIC). Export of light carbon from the photic zone lowers $\sum CO_2$ in the surface ocean and increases the $\delta^{13}C$ of DIC. Weakening of the biological pump leads to a surplus of light carbon in the surface ocean, higher atmospheric CO_2 levels, and a decrease in $\delta^{13}C$-CO_2. Accordingly, the $\delta^{13}C$ of the intermediate-depth ocean should increase in response to the decreased export of ^{13}C-depleted organic matter from the euphotic zone.

We evaluate the biological pump hypothesis using high-resolution planktonic and benthic foraminiferal $\delta^{13}C$ records. We use the planktonic records to reconstruct the $\delta^{13}C$ of DIC of the surface ocean, while the benthic records are used to estimate the $\delta^{13}C$ of DIC at approximately 1000 m water depth (Figure 1). Carbon isotope minima occurred at the surface and mid-depths during HS1 [*Ninnemann and Charles*, 1997; *Curry and Crowley*, 1987; *Spero and Lea*, 2002; *Oppo and Fairbanks*, 1989], with the largest anomalies being recorded from 1 to 2 km water depth in the high-latitude North Atlantic [*Oppo et al.*, 2015; *Rickaby and Elderfield*, 2005]. The overall spatial pattern of mid-depth (1500–2500 m) $\delta^{13}C$ anomalies appears to be largely driven by weakening of the AMOC, greater residence time of mid-depth waters in the Atlantic, and the accumulation of respired carbon [*Schmittner and Lund*, 2015].

Here we focus on paired surface and intermediate-depth $\delta^{13}C$ records to test whether upper ocean $\delta^{13}C$ gradients changed in response to variations in biological pump efficiency. A new high-resolution planktonic $\delta^{13}C$

Table 1. Summary of Cores and $\delta^{13}C$ Data Utilized in This Paper[a]

Location (See Figure 2)	Core	Depth (m)	Foraminifera Species		HS1 $\delta^{13}C$ Shift (‰)		HS1 $\Delta\delta^{13}C$ (‰)
			Planktonic	Benthic	Planktonic	Benthic	
1: Chatham Rise, Southern Ocean	MD97-2120	1210	*G. bulloides*	*Cibicidoides* spp.	−0.5	+0.4	−0.9
2: Australian Margin, SW Pacific	FR1/97 GC-12	990	*G. sacculifer*	*Cibicidoides* spp.	−0.5	+0.4	−0.9
			G. menardii		−0.5		−0.9
3: Eastern Equatorial Pacific	V19-27	1373	*G. sacculifer*	*C. wuellerstorfi*	−0.4	+0.2	−0.6
4: Brazil Margin, SW Atlantic	KNR159-5-78GGC[b]	1829[d]	*N. dutertrei*		−0.7		−0.9
	KNR159-5-90GGC[c]	1105		*Cibicidoides* spp.		+0.2	

[a]References are as follows: MD97-2120 [*Pahnke and Zahn*, 2005], FR1/97 GC-12 [*Bostock et al.*, 2004], V19-27 (planktonic record [*Koutavas and Lynch-Stieglitz*, 2003] and benthic record [*Mix et al.*, 1991]), KNR159-5-78GGC (planktonic record (this study) and age model [*Tessin and Lund*, 2013]), KNR159-5-90GGC (benthic record [*Curry and Oppo*, 2005] and age model [*Lund et al.*, 2015]).
[b]Planktonic record.
[c]Benthic record
[d]Core used for planktonic record only

time series was generated for the Brazil Margin, Southwest Atlantic (core KNR159-5-78GGC), for comparison to a published benthic $\delta^{13}C$ record from the same location (Location 4, Figure 1a) [*Tessin and Lund*, 2013; *Curry and Oppo*, 2005; *Lund et al.*, 2015]. We also examine planktonic and benthic records from three additional sites in the Southern and Pacific Oceans [*Pahnke and Zahn*, 2005; *Bostock et al.*, 2004; *Koutavas and Lynch-Stieglitz*, 2003; *Mix et al.*, 1991] (Table 1 and Figure 1a). Of the four locations, three are within the core of Antarctic Intermediate Water (AAIW) today, while one is located along its lower boundary (Figure 1b).

A weakened biological pump during HS1 would result in negative $\delta^{13}C$ anomalies in the surface ocean and positive $\delta^{13}C$ anomalies at intermediate depths, where the majority of organic matter remineralization occurs [*Kroopnick*, 1985]. Thus, the upper ocean vertical $\delta^{13}C$ gradient should decrease with reduced biological export production. We evaluate the $\delta^{13}C$ records in the context of results from a model simulation where variable AMOC strength influences biological pump efficiency and the oceanic $\delta^{13}C$ tracer field [*Schmittner and Lund*, 2015]. We also consider whether air-sea gas exchange could influence surface and intermediate-depth $\delta^{13}C$ during HS1 through temperature-dependent fractionation. Finally, we examine the $\delta^{13}C$ trends during the Bølling-Allerød (B-A: 12.9–14.5 kyr B.P.) and Younger Dryas (YD: 11.7–12.9 kyr B.P.) to determine whether there is evidence of biological pump variability during these time intervals. Proxy records suggest that the AMOC strengthened during the B-A and weakened again during the YD [*Chen et al.*, 2015; *McManus et al.*, 2004]. Therefore, the upper ocean vertical $\delta^{13}C$ gradient should increase during the B-A and decrease again during the YD.

2. Methods

Planktonic $\delta^{13}C$ results for core KNR159-5-78GGC are based on *Neogloboquadrina dutetrei* from the $>350\,\mu m$ size fraction that lacked evidence for secondary crusting. To minimize noise in the $\delta^{13}C$ time series, we crushed and homogenized 4–8 *N. dutetrei* tests from each sample and then ran four separate aliquots of powder to determine the mean $\delta^{13}C$ at each stratigraphic level. Analyses were run on a Finnigan MAT 253 triple-collector gas source mass spectrometer coupled to a Finnigan Kiel automated carbonate device at the University of Michigan's Stable Isotope Laboratory. Isotope values were corrected to Vienna Pee Dee Belemnite by using National Bureau of Standards 19 ($n = 26$, $\delta^{13}C = 1.94 \pm 0.05$‰, $\delta^{18}O = -2.24 \pm 0.06$‰). The other $\delta^{13}C$ records presented here are from the published literature. Table 1 lists the cores from which the records were derived, along with the planktonic and benthic species used to create the $\delta^{13}C$ time series. Specific methodologies for the published records can be found in the original citations (Table 1). The radiocarbon-based age model for each core was updated by using Calib 7.1 (http://calib.qub.ac.uk/calib/) and site-specific ΔR values (Table S1 in the supporting information shows the updated age models and ΔR values). Ages for samples between the calibrated dates were determined by linear interpolation.

The vertical gradient between surface and intermediate-depth $\delta^{13}C$ ($\Delta\delta^{13}C$) was determined by subtracting benthic $\delta^{13}C$ from planktonic $\delta^{13}C$ in each core. For Chatham Rise core MD97-2120 (Figure 2a) and Australian Margin core FR1/97 GC12 (Figure 2b), planktonic and benthic analyses were performed on the same

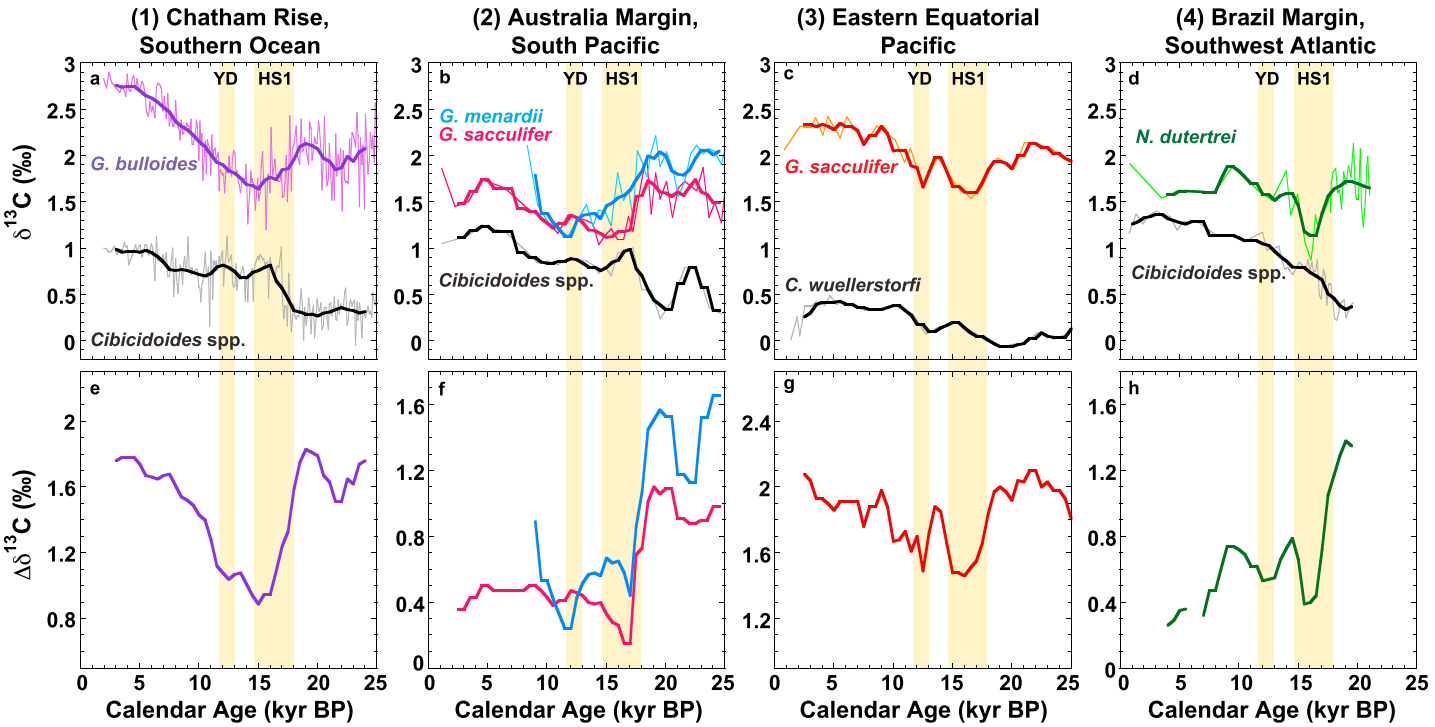

Figure 2. Records of $\delta^{13}C$ and $\Delta\delta^{13}C$ across the last deglaciation. (a–d) Planktonic $\delta^{13}C$ (colors) and benthic $\delta^{13}C$ records (black). Numbered locations correspond to those in Figure 1a and Table 1. The thick line is the 2 kyr running mean. Two per mil has been added to the *G. bulloides* data in (a) to correct for the empirically derived offset between shell $\delta^{13}C$ and $\delta^{13}C_{DIC}$ for this species [*Spero and Lea*, 1996]. (e–h) $\Delta\delta^{13}C$ for the corresponding $\delta^{13}C$ records in the top figures. $\Delta\delta^{13}C$ is computed as the difference between the planktonic (surface ocean) and benthic (intermediate depth) records. Heinrich Stadial 1 (HS1) and the Younger Dryas (YD) are denoted with beige bars. At all four locations, planktonic $\delta^{13}C$ decreases and benthic $\delta^{13}C$ increases across HS1, corresponding to a decrease in the upper ocean vertical $\delta^{13}C$ gradient ($\Delta\delta^{13}C$) of 0.6‰ to 0.9‰.

stratigraphic levels, so benthic $\delta^{13}C$ values were simply subtracted from planktonic $\delta^{13}C$ values for each interval. For core V19-27 in the Eastern Equatorial Pacific (EEP) (Figure 2c), planktonic and benthic $\delta^{13}C$ analyses were performed on different stratigraphic intervals. We therefore interpolated the planktonic and benthic $\delta^{13}C$ to common 1 kyr increments prior to calculating $\Delta\delta^{13}C$. At the Brazil Margin, the planktonic $\delta^{13}C$ record is from core KNR159-5-78GGC, while the benthic $\delta^{13}C$ record is from KNR159-5-90GGC (Figure 2d). For both cores, the $\delta^{13}C$ records were interpolated to a 0.25 kyr time step, the average deglacial sampling interval for each time series, before calculating $\Delta\delta^{13}C$.

The modeling results are site-specific vertical profiles generated in the 0.15 Sverdrup (Sv) freshwater hosing experiment described in *Schmittner and Lund* [2015] (Figure 3). The $\delta^{13}C$ anomalies represent the $\delta^{13}C$ difference between year 2500 of the 0.15 Sv experiment and a control run with no freshwater forcing, at the locations of the cores listed in Table 1. The results are based on the Model of Ocean Biogeochemistry and Isotopes (MOBI 1.4), a coupled climate-biogeochemical model that includes cycling of ^{13}C and ^{12}C. MOBI is embedded in the University of Victoria climate model of intermediate complexity version 2.9 and run to a preindustrial equilibrium [*Schmittner and Lund*, 2015]. Freshwater is input to the North Atlantic between 45–60°N and 60–0°W and occurs for 400 years at the beginning of the ~3500 year long simulation.

3. Results and Discussion

The planktonic and benthic records at all four locations display similar trends across the last deglaciation, with abrupt decreases and increases in $\delta^{13}C$, respectively, at the onset of HS1 (Figure 2 and Table 1). The planktonic records suggest that the $\delta^{13}C$ of surface ocean DIC decreased by 0.4‰ to 0.7‰, while the benthic records indicate that the $\delta^{13}C$ of intermediate waters increased by 0.2‰ to 0.4‰. At the Chatham Rise,

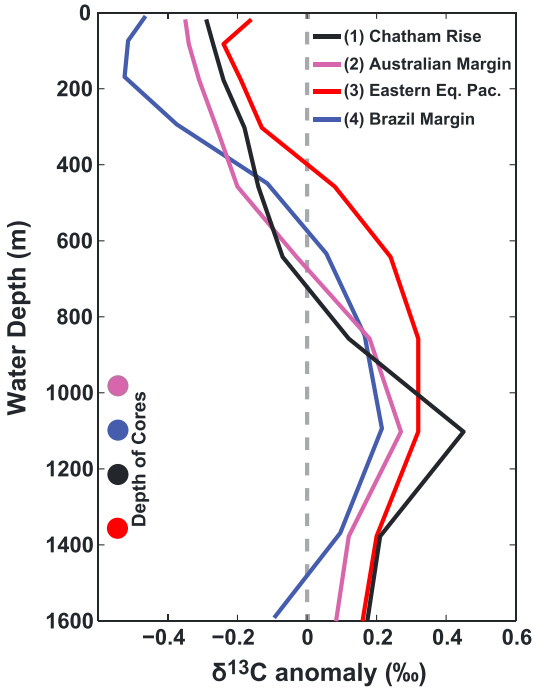

Figure 3. Simulated site-specific $\delta^{13}C$ anomalies for the locations shown in Figure 1. The $\delta^{13}C$ profiles represent the ocean's biogeochemical response to a weakened AMOC in the 0.15 Sv freshwater hosing experiment of *Schmittner and Lund* [2015]. The anomalies represent the $\delta^{13}C$ difference between year 2500 of the 0.15 Sv experiment and a control run with no freshwater forcing. A weakening of AMOC results in reduced biological pump efficiency, leading to negative surface ocean $\delta^{13}C$ anomalies due to accumulation of ^{12}C. Positive $\delta^{13}C$ anomalies at intermediate depths are due to the reduced export and remineralization of ^{13}C depleted organic matter from surface waters. The range of core depths is shown with circles along the *y* axis, with colors corresponding to each location.

Australian Margin, and Brazil Margin, the vertical $\delta^{13}C$ gradient ($\Delta\delta^{13}C$) decreased by ~0.9‰ during the transition from the Last Glacial Maximum (LGM) to HS1 (Figure 2 and Table 1). At the EEP site, $\Delta\delta^{13}C$ decreased by ~0.6‰, which is likely due to the core location being in an upwelling region (Figure 2 and Table 1). The results of *Schmittner and Lund* [2015] suggest that weakening of the biological pump increases the $\delta^{13}C$ of intermediate-depth water, which would be subsequently upwelled in the EEP, thereby minimizing the planktonic $\delta^{13}C$ signal.

To compare $\Delta\delta^{13}C$ variability across all four sites, we normalized the records by subtracting the average $\Delta\delta^{13}C$ value for the LGM (19.0–21.0 kyr B.P.) (Figure 4a). The vertical $\delta^{13}C$ gradient decreased synchronously at each location at the onset of HS1, increased during the B-A, and then decreased again during the YD. The only record that lacks a clear $\Delta\delta^{13}C$ minimum during the YD is the Australian Margin *Globorotalia menardii* record, which may be an artifact of the decreased sampling resolution in this core after HS1. The subtropical gyre records from the Brazil Margin and Australian Margin display a long-term decrease in $\Delta\delta^{13}C$, suggesting that there was an overall weakening of the biological pump at these sites between the LGM and late Holocene.

In order to isolate common millennial-scale variability, we detrended the $\Delta\delta^{13}C$ records (Figure 4b) and averaged the results to yield a $\Delta\delta^{13}C$ stack (Figure 4c). Creation of the stacked record facilitates comparison with atmospheric $\delta^{13}C$-CO_2 records, which the model results suggest should also be sensitive to the biological pump [*Schmittner and Lund*, 2015]. As in the simpler normalization case, the detrended records show coherent changes in $\Delta\delta^{13}C$ during HS1, the B-A, and YD (Figure 4b). In addition to the large decline in $\Delta\delta^{13}C$ at the onset of HS1, the stacked record shows an ~0.3‰ increase during the B-A and then a subtle decrease during the YD (Figure 4c). Although the YD signal approaches the uncertainty in the $\Delta\delta^{13}C$ estimate (0.07‰ across the YD), examination of the individual $\Delta\delta^{13}C$ records (Figures 2e–2h and 4b) suggests that the YD signal is robust.

Comparison of the foraminiferal $\delta^{13}C$ anomalies with simulated site-specific $\delta^{13}C$ results derived from an AMOC weakening experiment suggests that weakening of the biological pump is the most likely explanation of the upper ocean $\delta^{13}C$ signal during HS1 (Figure 3). The simulated reduction in biological pump efficiency results in $\delta^{13}C$ anomalies of -0.2‰ to -0.5‰ in the upper 150 m of the water column, the approximate depth habitat range of the planktonic foraminifera used for the $\delta^{13}C$ reconstructions (Figure 3). Maximum positive $\delta^{13}C$ anomalies occur at ~1 km water depth, similar to the depth of the corresponding sediment cores at each location. The simulated reduction in productivity results in the accumulation of ^{12}C in the surface ocean, while decreased organic matter export reduces the remineralization of ^{12}C at intermediate depths. A simulated minimum in phosphate concentrations occurs at depths similar to maximum positive

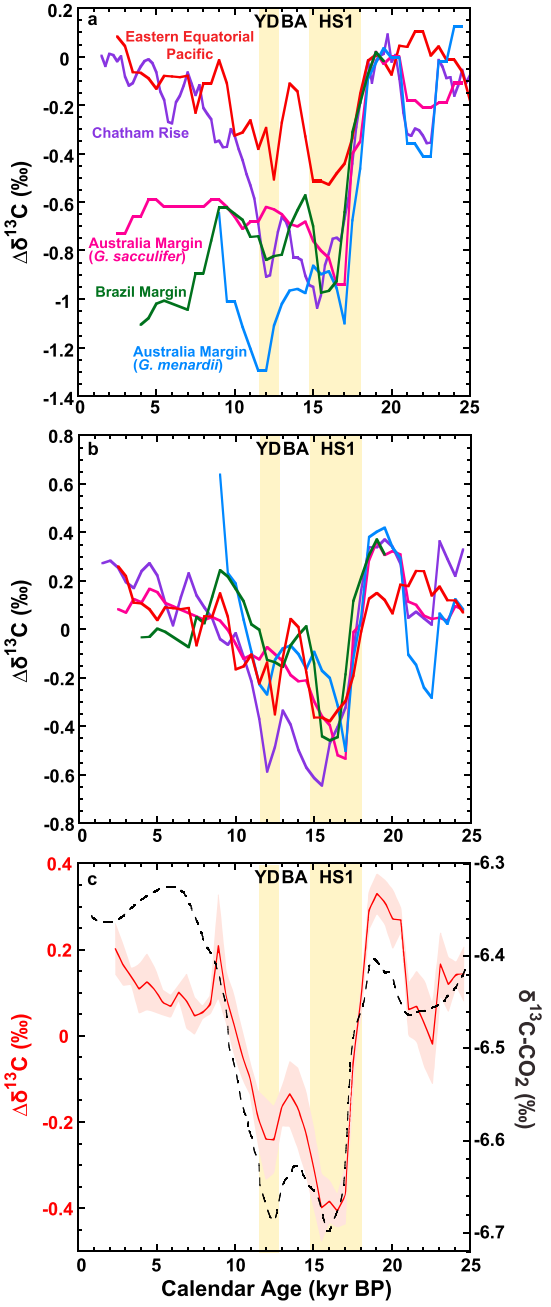

Figure 4. Deglacial $\Delta\delta^{13}C$ records showing millennial scale variability. (a) Compilation of $\Delta\delta^{13}C$ records shown in Figures 2e–2h normalized to their respective LGM average $\Delta\delta^{13}C$ (19–21 kyr B.P.) (the average LGM $\Delta\delta^{13}C$ value for each record was subtracted from the $\Delta\delta^{13}C$ record). (b) Compilation of detrended $\Delta\delta^{13}C$ records shown in Figures 2e–2h to remove glacial-interglacial $\delta^{13}C$ changes. (c) The average (i.e., stack) of the detrended $\Delta\delta^{13}C$ records in Figure 4b (red line) and the $\delta^{13}C$ of atmospheric CO_2 from *Schmitt et al.* [2012] (black dashed line). The pink error envelope on the stacked $\Delta\delta^{13}C$ record is the standard error. Note that the Australia Margin *G. menardii* record is significantly shorter than the other records, and thus, the detrended record is skewed to higher $\Delta\delta^{13}C$ values in the Holocene and accounts for the increase in the stacked $\Delta\delta^{13}C$ record at ~9 kyr B.P. HS1 and the YD are shown with beige bars, and the B-A is noted. Note the different *y* axis scales on Figures 4a–4c. The colors of the locations noted in Figure 4a are the same as in Figure 4b.

$\delta^{13}C$ anomalies, indicating that the $\delta^{13}C$ anomalies are the result of a weakening of the biological pump (Figure S2). The net effect of a weakened biological pump is to reduce the modeled vertical $\delta^{13}C$ gradient by 0.6‰ to 0.8‰ at each location, in good agreement with the observed change in $\Delta\delta^{13}C$ of 0.6‰ to 0.9‰ at the four core sites during HS1 (Figure 2).

Surface ocean $\delta^{13}C$ is affected not only by the biological pump but also by air-sea gas exchange. At isotopic equilibrium, warmer water has a lower $\delta^{13}C$ than cold water, with a thermodynamic slope of −0.1‰ per °C of warming [*Broecker and Maier-Reimer*, 1992]. Given the rise in sea surface temperature (SST) at many Southern Hemisphere locations early in the deglaciation [*Shakun et al.*, 2012], a portion of the negative planktonic $\delta^{13}C$ anomalies is likely due to warming (Figure S3). For example, the *Globigerina bulloides* Mg/Ca SST record from the same Chatham Rise core as the $\delta^{13}C$ time series in Figure 3 implies that SSTs increased 2°C to 3°C during HS1 [*Pahnke et al.*, 2003] (Figure S3). If surface waters were in equilibrium with the atmosphere, the thermodynamic effect could account for up to half of the 0.5‰ decrease in $\delta^{13}C$. The planktonic $\delta^{13}C$ records suggest that, on average, surface ocean $\delta^{13}C$ decreased by approximately 0.5‰ during HS1, approximately 0.2‰ more than the atmospheric $\delta^{13}C$ signal [*Bauska et al.*, 2016]. SSTs therefore likely modulated the biological pump effect, causing surface ocean $\delta^{13}C$ to be more depleted and atmospheric $\delta^{13}C$ to be more enriched than they would otherwise be. Note that warming temperatures cannot fully explain planktonic $\delta^{13}C$ anomalies during HS1; if this were the case, then the atmospheric $\delta^{13}C$ signal would be of opposite sign due to a decrease in air-sea fractionation [*Spero and Lea*, 2002].

While the biological pump and air-sea gas exchange exert the primary control on surface ocean $\delta^{13}C$, the carbon isotope signature of planktonic foraminifera can be offset from seawater $\delta^{13}C$ due to vital effects. These vital effects include foraminiferal respiration, photosynthetic fractionation by algal symbionts, and vertical migration [*Spero et al.*, 2003; *Spero and Lea*, 1996; *Curry and Crowley*, 1987; *Spero and Lea*, 1993]. Comparison of the records (Figures 2a–2d) derived from different species of planktonic foraminifera suggests that vital effects have little influence on the HS1 $\delta^{13}C$ anomalies. The Chatham Rise $\delta^{13}C$ time series is based on *G. bulloides*, a symbiont barren species, while the Australian Margin $\delta^{13}C$ record is based on *Globigerinoides sacculifer*, a symbiont bearing species, yet both show HS1 $\delta^{13}C$ anomalies of −0.5‰. Furthermore, a second record from the Australian Margin, based on the thermocline-dwelling species *G. menardii*, also shows a HS1 $\delta^{13}C$ anomaly of −0.5‰, identical to that of *G. sacculifer*. Although these results are spatially limited, other studies have found that different planktonic species yield similar magnitude $\delta^{13}C$ anomalies during the last deglaciation [*Spero et al.*, 2003; *Koutavas and Lynch-Stieglitz*, 2003; *Pena et al.*, 2008; *Carter et al.*, 2008; *Charles et al.*, 1996].

Prevailing hypotheses for the CO_2 rise during HS1 often invoke Southern Ocean processes. Specifically, invigorated upwelling in the Southern Ocean may have increased ventilation of the deep ocean and released glacially sequestered CO_2 and/or weakened the biological pump by breaking down stratification in the Southern Ocean [e.g., *Anderson et al.*, 2009; *Denton et al.*, 2010; *Skinner et al.*, 2010; *Toggweiler et al.*, 2006; *Tschumi et al.*, 2011]. A decrease in dust delivery near Antarctica may have contributed to a weaker biological pump in the Southern Ocean at the onset of HS1 by decreasing nutrient utilization [*Ziegler et al.*, 2013]. *Toggweiler et al.* [2006] argued that an increase in Southern Ocean wind forcing via a poleward shift in the midlatitude westerlies was responsible for releasing CO_2 from the deep ocean during HS1, although an unrealistically large (80%) increase in wind stress is needed to achieve this result [*Tschumi et al.*, 2011]. Furthermore, coarse-resolution models like those utilized in *Toggweiler et al.* [2006] and *Tschumi et al.* [2011] yield artificially large circulation responses due to their inability to resolve mesoscale eddies. In higher-resolution eddy-permitting models, increased poleward eddy fluxes largely compensate for enhanced equatorward Ekman transport due to a strengthening of the westerlies [*Farneti and Delworth*, 2010]. As a result, there is a greatly weakened deep ocean ventilation response to wind forcing in the Southern Ocean [*Farneti and Delworth*, 2010].

Based on evidence of widespread $\delta^{13}C$ minima in surface- and thermocline-dwelling foraminifera [*Oppo and Fairbanks*, 1989; *Curry and Crowley*, 1987; *Ninnemann and Charles*, 1997], *Spero and Lea* [2002] hypothesized that enhanced deep mixing around Antarctica upwelled CO_2 rich, $\delta^{13}C$-depleted water into the surface Southern Ocean. Atmospheric pCO_2 would rise and the $\delta^{13}C$ of CO_2 would decrease as CO_2-supersaturated waters outgassed to the atmosphere [*Spero and Lea*, 2002]. They also hypothesized that the light carbon signal would become entrained into Sub-Antarctic Mode Water (SAMW) and AAIW, allowing communication of the signal to lower latitudes.

The positive shift in benthic $\delta^{13}C$ at the four locations in our study is inconsistent with the *Spero and Lea* [2002] hypothesis. If AAIW was the primary carrier of light carbon from the Southern Ocean, one would expect to observe negative benthic foraminiferal $\delta^{13}C$ anomalies at the core sites, which are in the flow path of AAIW. The opposite signal is observed, however, with benthic $\delta^{13}C$ increasing across HS1. Air-sea gas exchange could potentially overprint a light carbon signature of water upwelled from the abyssal Southern Ocean through thermodynamic and gas exchange rate effects [*Lynch-Stieglitz et al.*, 1995]. The thermodynamic slope of −0.1‰ per °C of warming [*Broecker and Maier-Reimer*, 1992] is the maximum expected temperature effect because of the long (~10 year) equilibration time for $\delta^{13}C$ [*Broecker and Maier-Reimer*, 1992; *Schmittner et al.*, 2013] relative to the residence time of Antarctic surface waters (~2 years [*Gordon*, 1988]). Therefore, a 0.3‰ positive shift in benthic $\delta^{13}C$ would require both sufficient equilibration and a cooling of ~3°C in AAIW source regions. Such a change is unlikely given that SSTs warmed early in the deglaciation, including those in the main formation regions of AAIW (Figure S3). Instead, warming SSTs in AAIW source regions would act to decrease the $\delta^{13}C$ of AAIW, opposite of the observed trend (Figure 2). Alternatively, a doubling of the gas exchange rate could potentially increase the preformed $\delta^{13}C$ of AAIW by 0.2‰ to 0.4‰ [*Broecker and Maier-Reimer*, 1992]. Given the observed warming, this would be the minimum shift in gas exchange rate required to account for the positive benthic $\delta^{13}C$ anomalies.

Our results are inconsistent with greater upwelling in the Southern Ocean at the onset of HS1, as it is difficult to imagine a scenario in which upwelling strengthened but did not transfer a light carbon signature to AAIW/SAMW. Additionally, benthic foraminiferal $\delta^{18}O$, $\delta^{13}C$, and B/Ca records suggest that abyssal circulation

began to shift during the B-A, well after the initial increase in CO_2 [*Lund et al.*, 2015; *Waelbroeck et al.*, 2011; *Yu et al.*, 2014; *Roberts et al.*, 2016]. Furthermore, deep-sea coral records from the Southern Ocean lack evidence for a breakdown in stratification during HS1 [*Chen et al.*, 2015]. These studies suggest that there was a role for Southern Ocean upwelling of CO_2-rich deep waters, but not until the B-A, more than 2 kyr after the initial rise in atmospheric CO_2. A decrease in dust delivery to the Southern Ocean at the onset of HS1 may have weakened the biological pump on a regional basis due to a decrease in iron fertilization [*Bauska et al.*, 2016; *Martínez-García et al.*, 2014; *Ziegler et al.*, 2013], but such a process would unlikely account for the coherent changes in surface and intermediate-depth $\delta^{13}C$ at locations in the Southern Ocean, subtropical Atlantic and Pacific, and the equatorial Pacific (Figures 2 and 4). Although a decrease in iron fertilization may have contributed to the HS1 CO_2 rise, this mechanism has not yet been quantitatively evaluated in model simulations. An AMOC-driven increase in atmospheric CO_2 during HS1 is consistent with the two-mode explanation for deglacial CO_2 rise described by *Galbraith and Jaccard* [2015]. Under this scenario, LGM to Holocene changes in the biological pump are driven by variations in iron fertilization and ocean ventilation, while millennial-scale changes are driven by the AMOC.

If weakening of the biological pump during HS1 was driven by a collapse of the AMOC, as our data suggest, the upper ocean $\delta^{13}C$ gradient should also increase during the B-A when the AMOC strengthened [*Chen et al.*, 2015; *McManus et al.*, 2004]. The observed positive shift in $\Delta\delta^{13}C$ during the B-A (Figure 4c) is consistent with re-invigorated biological productivity, which would promote the export of light carbon from surface waters to intermediate depths and create a larger vertical $\delta^{13}C$ gradient. Furthermore, $\Delta\delta^{13}C$ decreased again during the YD (Figure 4), consistent with the expected pattern due to weakening of the AMOC. The $\Delta\delta^{13}C$ stack in Figure 4c represents the average upper ocean $\delta^{13}C$ gradient, which our model results show is highly sensitive to changes in the biological productivity. The overall agreement between the oceanic and ice core $\delta^{13}C$ records provides strong support for a biological pump driver of millennial-scale CO_2 variability during the last deglaciation.

4. Conclusions

The simplest explanation of the observed planktonic and benthic signals during HS1 and the YD is reduced efficiency of the biological pump, which would preferentially leave light carbon in the surface ocean and limit its export to intermediate depths. The change in biological pump efficiency was likely due to weakening of the AMOC, which increases the mean fraction of preformed phosphate in the global ocean, allowing CO_2 to accumulate in the surface ocean and atmosphere [*Schmittner and Lund*, 2015; *Ito and Follows*, 2005]. Furthermore, the $\delta^{13}C$ records are inconsistent with a Southern Ocean release of abyssal, $\delta^{13}C$ depleted CO_2 to the atmosphere during HS1. If this scenario was correct, benthic foraminiferal $\delta^{13}C$ from regions influenced by AAIW should decrease early in the deglaciation, which is opposite of the reconstructed signal at multiple AAIW-sensitive sites. Together with surface ocean carbon isotope minima, the intermediate-depth signal is most easily explained by reduced export of light carbon from the euphotic zone. When AMOC strengthened at the end of HS1, our results suggest that biological pump efficiency increased, as evidenced by strengthening of the upper ocean $\delta^{13}C$ gradient. The similar timing of AMOC proxies and $\Delta\delta^{13}C$ during HS1, the B-A, and YD provides strong evidence for a North Atlantic driver of millennial-scale changes in biological pump variability across the last deglaciation. Furthermore, our oceanic $\Delta\delta^{13}C$ reconstructions are similar to the $\delta^{13}C$ of atmospheric CO_2, consistent with model results that show reduced AMOC strength and biological pump efficiency results in the accumulation of light carbon in the surface ocean and atmosphere [*Schmittner and Lund*, 2015]. These findings have important implications for understanding glacial terminations and the drivers of carbon cycle variability over long time scales, especially the potential for AMOC to alter the oceanic nutrient budget. Weakening of the AMOC and biological pump likely triggered rising atmospheric CO_2 during HS1 and the YD and appears to be a key factor in the Earth's transition from a glacial to interglacial climate state.

Acknowledgments

We would like to thank Lora Wingate at the University of Michigan for stable isotope analyses of *N. dutetrei* from core KNR159-5-78GGC. We are grateful to the WHOI core laboratory for core collection and archiving. We thank the two anonymous reviewers and the editor for their helpful comments. We would also like to acknowledge the scientists responsible for generating the data compiled in this manuscript, including Helen Bostock, Tom Koutavas, Bill Curry, Alan Mix, and Katharina Pahnke. D.C.L. acknowledges support from the NSF grant OCE-1003500 and the University of Connecticut. A.S. acknowledges support from the NSF grant OCE-1131834. The new Brazil Margin $\delta^{13}C$ data will be made available on the NOAA National Center for Environmental Information-Paleoclimatology website (https://www.ncdc.noaa.gov/data-access/paleoclimatology-data).

References

Anderson, R. F., S. Ali, L. I. Bradtmiller, S. H. H. Nielsen, M. Q. Fleisher, B. E. Anderson, and L. H. Burckle (2009), Wind-driven upwelling in the Southern Ocean and the deglacial rise in atmospheric CO_2, *Science*, *323*, 1443–1448.

Barker, S., P. Diz, M. J. Vautravers, J. Pike, G. Knorr, I. R. Hall, and W. S. Broecker (2009), Interhemispheric Atlantic seesaw response during the last deglaciation, *Nature*, *457*(7233), 1097–1102.

Bauska, T. K., D. Baggenstos, E. J. Brook, A. C. Mix, S. A. Marcott, V. V. Petrenko, H. Schaefer, J. P. Severinghaus, and J. E. Lee (2016), Carbon isotopes characterize rapid changes in atmospheric carbon dioxide during the last deglaciation, *Proc. Natl. Acad. Sci.*, *113*(13), 3465–3470, doi:10.1073/pnas.1513868113.

Bostock, H. C., B. N. Opdyke, M. K. Gagan, and L. K. Fifield (2004), Carbon isotope evidence for changes in Antarctic Intermediate Water circulation and ocean ventilation in the southwest Pacific during the last deglaciation, *Paleoceanography*, *19*, PA4013, doi:10.1029/2004PA001047.

Broecker, W. S., and E. Maier-Reimer (1992), The influence of air and sea exchange on the carbon isotope distribution in the sea, *Global Biogeochem. Cycles*, *6*(3), 315–320, doi:10.1029/92GB01672.

Carter, L., B. Manighetti, G. Ganssen, and L. Northcote (2008), Southwest Pacific modulation of abrupt climate change during the Antarctic Cold Reversal–Younger Dryas, *Palaeogeogr. Palaeoclimatol. Palaeoecol.*, *260*(1–2), 284–298, doi:10.1016/j.palaeo.2007.08.013.

Charles, C. D., J. Lynch-Stieglitz, U. S. Ninnemann, and R. G. Fairbanks (1996), Climate connections between the hemisphere revealed by deep sea sediment core/ice core correlations, *Earth Planet. Sci. Lett.*, *142*(1), 19–27, doi:10.1016/0012-821X(96)00083-0.

Chen, T., L. F. Robinson, A. Burke, J. Southon, P. Spooner, P. J. Morris, and H. C. Ng (2015), Synchronous centennial abrupt events in the ocean and atmosphere during the last deglaciation, *Science*, *349*(6255), 1537–1541, doi:10.1126/science.aac6159.

Curry, W. B., and T. J. Crowley (1987), The $\delta^{13}C$ of equatorial Atlantic surface waters: Implications for Ice Age pCO_2 levels, *Paleoceanography*, *2*(5), 489–517, doi:10.1029/PA002i005p00489.

Curry, W. B., and D. W. Oppo (2005), Glacial water mass geometry and the distribution of $\delta^{13}C$ of ΣCO_2 in the western Atlantic Ocean, *Paleoceanography*, *20*, PA1017, doi:10.1029/2004PA001021.

Denton, G. H., R. F. Anderson, J. R. Toggweiler, R. L. Edwards, J. M. Schaefer, and A. E. Putnam (2010), The last glacial termination, *Science*, *328*(5986), 1652–1656.

Farneti, R., and T. L. Delworth (2010), The role of mesoscale eddies in the remote oceanic response to altered Southern Hemisphere winds, *J. Phys. Oceanogr.*, *40*(10), 2348–2354, doi:10.1175/2010JPO4480.1.

Galbraith, E. D., and S. L. Jaccard (2015), Deglacial weakening of the oceanic soft tissue pump: Global constraints from sedimentary nitrogen isotopes and oxygenation proxies, *Quat. Sci. Rev.*, *109*, 38–48.

Gherardi, J., L. Labeyrie, S. Nave, R. Francois, J. F. McManus, and E. Cortijo (2009), Glacial-interglacial circulation changes inferred from $^{231}Pa/^{230}Th$ sedimentary record in the North Atlantic region, *Paleoceanography*, *24*, PA2204, doi:10.1029/2008PA001696.

Gordon, A. L. (1988), Spatial and temporal variability within the southern ocean, in *Antarctic Ocean and Resources Variability*, edited by Dietrich Sahrhage, pp. 41–56, Springer, Berlin.

Ito, T., and M. J. Follows (2005), Preformed phosphate, soft tissue pump and atmospheric CO_2, *J. Mar. Res.*, *63*(4), 813–839, doi:10.1357/0022240054663231.

Koutavas, A., and J. Lynch-Stieglitz (2003), Glacial-interglacial dynamics of the eastern equatorial Pacific cold tongue-Intertropical Convergence Zone system reconstructed from oxygen isotope records, *Paleoceanography*, *18*(4), 1089, doi:10.1029/2003PA000894.

Kroopnick, P. M. (1985), The distribution of ^{13}C of ΣCO_2 in the world oceans, *Deep Sea Res., Part A*, *32*(1), 57–84, doi:10.1016/0198-0149(85)90017-2.

Lamy, F., J. Kaiser, H. W. Arz, D. Hebbeln, U. Ninnemann, O. Timm, A. Timmermann, and J. R. Toggweiler (2007), Modulation of the bipolar seesaw in the Southeast Pacific during Termination 1, *Earth Planet. Sci. Lett.*, *259*(3–4), 400–413, doi:10.1016/j.epsl.2007.04.040.

Lund, D. C., A. C. Tessin, J. L. Hoffman, and A. Schmittner (2015), Southwest Atlantic water mass evolution during the last deglaciation, *Paleoceanography*, *30*, 477–494, doi:10.1002/2014PA002657.

Lynch-Stieglitz, J., T. F. Stocker, W. S. Broecker, and R. G. Fairbanks (1995), The influence of air-sea exchange on the isotopic composition of oceanic carbon: Observations and modeling, *Global Biogeochem. Cycles*, *9*(4), 653–665, doi:10.1029/95GB02574.

Marcott, S. A., et al. (2014), Centennial-scale changes in the global carbon cycle during the last deglaciation, *Nature*, *514*(7524), 616–619.

Martínez-García, A., D. M. Sigman, H. Ren, R. F. Anderson, M. Straub, D. A. Hodell, S. L. Jaccard, T. I. Eglinton, and G. H. Haug (2014), Iron fertilization of the Subantarctic Ocean during the last ice age, *Science*, *343*(6177), 1347–1450.

McManus, J. F., R. Francois, J. Gherardi, L. D. Keigwin, and S. Brown-Leger (2004), Collapse and rapid resumption of Atlantic meridional circulation linked to deglacial climate changes, *Nature*, *428*(6985), 834–837.

Mix, A. C., N. G. Pisias, R. Zahn, W. Rugh, C. Lopez, and K. Nelson (1991), Carbon 13 in Pacific deep and intermediate waters, 0–370 ka: Implications for ocean circulation and Pleistocene CO_2, *Paleoceanography*, *6*(2), 205–226, doi:10.1029/90PA02303.

Ninnemann, U. S., and C. D. Charles (1997), Regional differences in Quaternary subantarctic nutrient cycling: Link to intermediate and deep water ventilation, *Paleoceanography*, *12*(4), 560–567, doi:10.1029/97PA01032.

Oppo, D. W., and R. G. Fairbanks (1989), Carbon isotope composition of tropical surface water during the past 22,000 years, *Paleoceanography*, *4*(4), 333–351, doi:10.1029/PA004i004p00333.

Oppo, D. W., W. B. Curry, and J. F. McManus (2015), What do benthic $\delta^{13}C$ and $\delta^{18}O$ data tell us about Atlantic circulation during Heinrich Stadial 1?, *Paleoceanography*, *30*, 353–368, doi:10.1002/2014PA002667.

Pahnke, K., and R. Zahn (2005), Southern Hemisphere water mass conversion linked with North Atlantic climate variability, *Science*, *307*(5716), 1741–1746, doi:10.1126/science.1102163.

Pahnke, K., R. Zahn, H. Elderfield, and M. Schulz (2003), 340,000-year centennial-scale marine record of Southern Hemisphere climatic oscillation, *Science*, *301*(5635), 948–952, doi:10.1126/science.1084451.

Pena, L. D., I. Cacho, P. Ferretti, and M. A. Hall (2008), El Niño–Southern Oscillation–like variability during glacial terminations and interlatitudinal teleconnections, *Paleoceanography*, *23*, PA3101, doi:10.1029/2008PA001620.

Rickaby, R. E. M., and H. Elderfield (2005), Evidence from the high-latitude North Atlantic for variations in Antarctic Intermediate water flow during the last deglaciation, *Geochem. Geophys. Geosyst.*, *6*, Q05001, doi:10.1029/2004GC000858.

Roberts, J., J. Gottschalk, L. C. Skinner, V. L. Peck, S. Kender, H. Elderfield, C. Waelbroeck, N. Vázquez Riveiros, and D. A. Hodell (2016), Evolution of South Atlantic density and chemical stratification across the last deglaciation, *Proc. Natl. Acad. Sci.*, *113*(3), 514–519, doi:10.1073/pnas.1511252113.

Schmitt, J., et al. (2012), Carbon isotope constraints on the deglacial CO_2 rise from ice cores, *Science*, *336*(6082), 711–714, doi:10.1126/science.1217161.

Schmittner, A. (2005), Decline of the marine ecosystem caused by a reduction in the Atlantic overturning circulation, *Nature*, *434*, 628–633.

Schmittner, A., and E. D. Galbraith (2008), Glacial greenhouse-gas fluctuations controlled by ocean circulation changes, *Nature*, *456*(7220), 373–376.

Schmittner, A., and D. C. Lund (2015), Early deglacial Atlantic overturning decline and its role in atmospheric CO_2 rise inferred from carbon isotopes ($\delta^{13}C$), *Clim. Past*, *11*(2), 135–152, doi:10.5194/cp-11-135-2015.

Schmittner, A., N. Gruber, A. C. Mix, R. M. Key, A. Tagliabue, and T. K. Westberry (2013), Biology and air–sea gas exchange controls on the distribution of carbon isotope ratios ($\delta^{13}C$) in the ocean, *Biogeosciences*, *10*(9), 5793–5816, doi:10.5194/bg-10-5793-2013.

Shakun, J. D., P. U. Clark, F. He, S. A. Marcott, A. C. Mix, Z. Liu, B. Otto-Bliesner, A. Schmittner, and E. Bard (2012), Global warming preceded by increasing carbon dioxide concentrations during the last deglaciation, *Nature*, *484*(7392), 49–54.

Skinner, L. C., S. Fallon, C. Waelbroeck, E. Michel, and S. Barker (2010), Ventilation of the Deep Southern Ocean and Deglacial CO_2 Rise, *Science*, *328*, 1147–1151.

Spero, H. J., and D. W. Lea (1993), Intraspecific stable isotope variability in the planktic foraminifera Globigerinoides sacculifer: Results from laboratory experiments, *Mar. Micropaleontol.*, *22*(3), 221–234, doi:10.1016/0377-8398(93)90045-Y.

Spero, H. J., and D. W. Lea (1996), Experimental determination of stable isotope variability in *Globigerina bulloides*: Implications for paleoceanographic reconstructions, *Mar. Micropaleontol.*, *28*(3–4), 231–246, doi:10.1016/0377-8398(96)00003-5.

Spero, H. J., and D. W. Lea (2002), The cause of carbon isotope minimum events on glacial terminations, *Science*, *296*(5567), 522–525, doi:10.1126/science.1069401.

Spero, H. J., K. M. Mielke, E. M. Kalve, D. W. Lea, and D. K. Pak (2003), Multispecies approach to reconstructing eastern equatorial Pacific thermocline hydrography during the past 360 kyr, *Paleoceanography*, *18*(1), 1022, doi:10.1029/2002PA000814.

Talley, L. D. (2008), Freshwater transport estimates and the global overturning circulation: Shallow, deep and throughflow components, *Prog. Oceanogr.*, *78*(4), 257–303, doi:10.1016/j.pocean.2008.05.001.

Tessin, A. C., and D. C. Lund (2013), Isotopically depleted carbon in the mid-depth South Atlantic during the last deglaciation, *Paleoceanography*, *28*, 296–306, doi:10.1002/palo.20026.

Toggweiler, J. R., J. L. Russell, and S. R. Carson (2006), Midlatitude westerlies, atmospheric CO_2, and climate change during the ice ages, *Paleoceanography*, *21*, PA2005, doi:10.1029/2005PA001154.

Tschumi, T., F. Joos, M. Gehlen, and C. Heinze (2011), Deep ocean ventilation, carbon isotopes, marine sedimentation and the deglacial CO_2 rise, *Clim. Past*, *7*(3), 771–800, doi:10.5194/cp-7-771-2011.

Waelbroeck, C., L. C. Skinner, L. Labeyrie, J.-C. Duplessy, E. Michel, N. Vazquez Riveiros, J.-M. Gherardi, and F. Dewilde (2011), The timing of deglacial circulation changes in the Atlantic, *Paleoceanography*, *26*, PA3213, doi:10.1029/2010PA002007.

Yu, J., R. F. Anderson, Z. Jin, L. Menviel, F. Zhang, F. J. Ryerson, and E. J. Rohling (2014), Deep South Atlantic carbonate chemistry and increased interocean deep water exchange during last deglaciation, *Quat. Sci. Rev.*, *90*, 80–89, doi:10.1016/j.quascirev.2014.02.018.

Ziegler, M., P. Diz, I. R. Hall, and R. Zahn (2013), Millennial-scale changes in atmospheric CO_2 levels linked to the Southern Ocean carbon isotope gradient and dust flux, *Nat. Geosci.*, *6*, 457–461.

Zweng, M. M., et al. (2013), World ocean atlas 2013, volume 2: Salinity, in *NOAA Atlas NESDIS*, 74th ed., edited by S. Levitus and A. Mishonov, NOAA, Washington, D. C.